Supplemental Material for

"Mode-resolved reciprocal space mapping of electron-phonon interaction in the Weyl semimetal candidate Td-WTe$_2$"

Petra Hein,[1] Stephan Jauernik,[1] Hermann Erk,[1] Lexian Yang,[2]

Yanpeng Qi,[3,4] Yan Sun,[4] Claudia Felser,[4] and Michael Bauer[1]

[1]*Institute of Experimental and Applied Physics,*

University of Kiel, Leibnizstr. 19, D-24118 Kiel, Germany

[2]*State Key Laboratory of Low Dimensional Quantum Physics,*

Collaborative Innovation Center of Quantum Matter and Department of Physics,

Tsinghua University, Beijing 100084, P. R. China

[3]*School of Physical Science and Technology,*

*ShanghaiTech University, Shanghai 201210, China*

[4]*Max Planck Institute for Chemical Physics of Solids,*

Nöthnitzer Str. 40, D-01187 Dresden, Germany

(Dated: January 23, 2020)

SUPPLEMENTARY NOTE 1: LONG-LIVED SPECTRAL CHANGES

Time-resolved ARPES results covering an extended pump-probe delay range up to $\Delta t = 400\,\text{ps}$ are compiled in Fig. S.1. Figure S.1(a) shows a ground state ARPES intensity map recorded 10 ps before the optical excitation in comparison to a difference intensity map at $\Delta t = 400\,\text{ps}$. The presence of red and blue areas in the difference intensity map indicates that at this time delay the system has still not reached its initial equilibrium state. To further illustrate the long-lived spectral changes, we analyzed the transient peak shifts of three bands labeled (I), (II), and (III) in Fig. S.1(a). The peak positions are determined from Gaussian fits to the transient EDCs of the respective bands. The results of the analysis are summarized in Fig. S.1(b). All bands exhibit rapid energy shifts between $7\,\text{meV}$ and $11\,\text{meV}$ at time zero followed by an exponential relaxation on a few picosecond time scale. We assign these dynamics to band renormalization processes in response to the excitation and subsequent relaxation of hot carriers. At $\Delta t \approx 5\,\text{ps}$, the energy of band (II) has relaxed
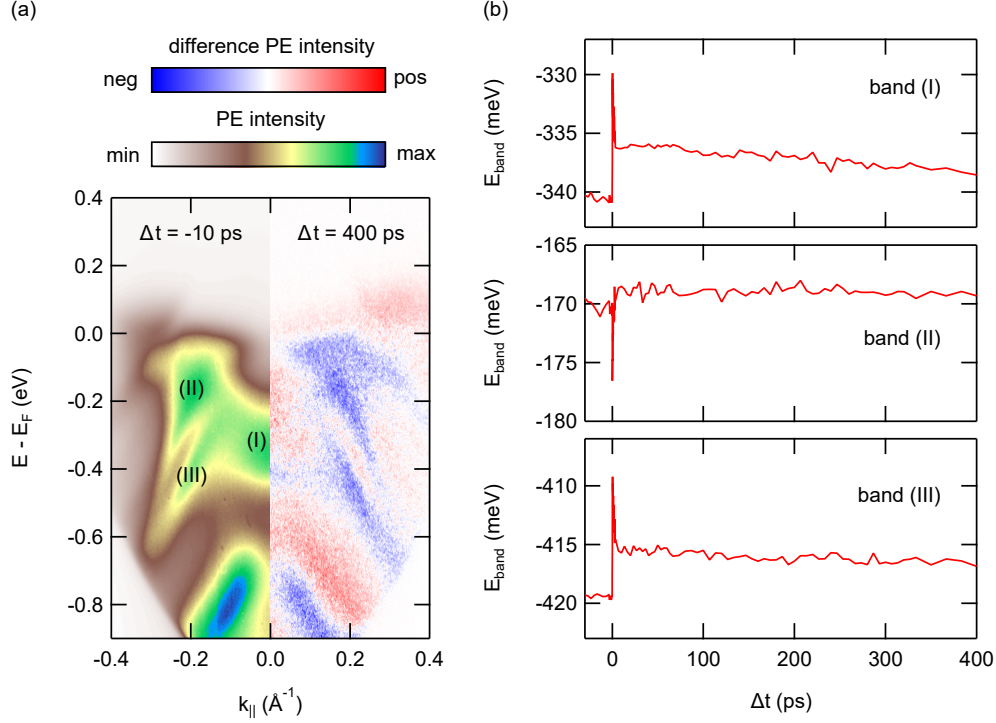
Supplementary Fig. S.1. Long-lived spectral changes in the TRARPES data of Td-WTe$_2$. (a) ARPES intensity map recorded at $\Delta t = -10$ ps in comparison to a difference intensity map at $\Delta t = 400$ ps. (b) Peak energies of the three bands indicated in (a) as a function of Δt.

back to nearly its initial value, while bands (I) and (III) still exhibit clear energy offsets of ≈ 4 meV. At the maximum time delay of 400 ps, the two bands still show offsets of ≈ 2 meV. Other time-resolved studies reported on similar long-lived spectral changes in Td-WTe$_2$ [? ?]. Their persistence was associated with heat diffusion out of the excitation volume on a characteristic time scale of several nanoseconds [?].

SUPPLEMENTARY NOTE 2: SAMPLING FREQUENCIES

To be able to track the high- as well as the low-frequency coherent phonon-induced oscillations, we recorded TRARPES data sets using two different sampling rates. A sampling rate of 60 THz enabled us to measure at the required resolution the beating signal caused by the superposition of coherent phonon modes with frequencies between 2.41 THz ($T = 415$ fs) and 6.35 THz ($T = 157$ fs) [cf. Fig. **??**(c) in the main text]. For these measurements, the total delay range was restricted to 3 ps to keep the overall data acquisition time at an
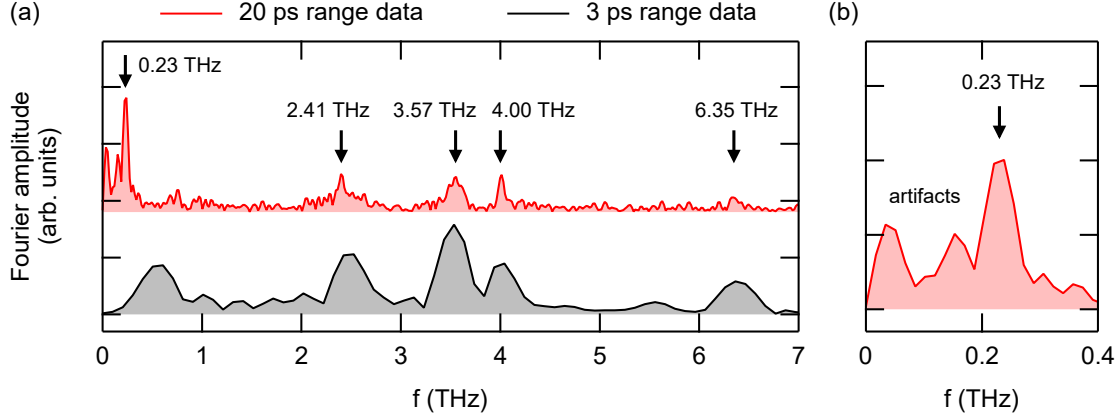
Supplementary Fig. S.2. Fourier amplitude spectra of the PE intensity transients shown in Figs. **??**(c) and **??**(d) of the main text. (a) Comparison of the Fourier amplitude spectra of the 3 ps range data and the 20 ps range data. (b) Close-up of the low-frequency range of the 20 ps range data.

acceptable level. The low-frequency interlayer shear mode exhibits a period of $T = 4.35$ ps so that a significantly longer delay range had to be chosen. For these measurements, the total delay range was set to 20 ps. As the highest energy phonon branch in Td-WTe$_2$ exhibits a frequency of approximately 7.2 THz [**? ?**], we chose for these measurements a sampling rate of 15 THz [cf. Fig. **??**(d) in the main text]. In this way, aliasing distortions of the transients by the high-frequency components are avoided.

While the 20 ps range data shows a reduced time-domain resolution in comparison to the 3 ps range data, it features a higher frequency resolution. The frequency increment of the Fourier analysis, given by the reciprocal total sampling time, is ≈ 0.3 THz and ≈ 0.05 THz for the 3 ps and 20 ps range data, respectively. Figure S.2(a) compares the Fourier amplitude spectra of the 3 ps and 20 ps range intensity transients shown in Figs. **??**(c) and **??**(d) of the main text. While the four high-frequency components are already evident in the amplitude spectrum of the 3 ps range data, their shape becomes much clearer in the amplitude spectrum of the 20 ps range data allowing for a more precise determination of the peak positions. The 0.23 THz interlayer shear mode can only be resolved in the 20 ps range data set. Furthermore, we observe additional peaks at frequencies below 0.23 THz [see Fig. S.2(b)]. They do not match any of the predicted or observed phonon modes of Td-WTe$_2$ [**? ? ? ? ?**]. In contrast to the five main frequency peaks between 0.23 THz and 6.35 THz, the positions and

relative heights of these very-low frequency peaks are quite sensitive to the data analysis procedures, e.g., the delay range included in the analysis and the model function used for background subtraction. We therefore conclude that the appearance of these peaks arises from artifacts of the data analysis.

SUPPLEMENTARY NOTE 3: BACKGROUND CORRECTION OF PHOTOEMISSION TRANSIENTS

The temporal evolution of the transient PE signal of Td-WTe$_2$ is mainly determined by contributions from the hot carrier dynamics and the coherent phonon oscillations. To separate the two signal contributions, we fitted the PE intensity transients with a model function accounting for the carrier population dynamics. Subtraction of the fitting result from the experimental data enables us to extract the pure oscillatory part of the signal. For the fits, we used the following function:

$$I(\Delta t) = \begin{cases} I_{01}, & \Delta t < t_0 \\ I_{02} + A_1 \cdot \exp\left(-\frac{\Delta t - t_0}{\tau_1}\right) + A_2 \cdot \exp\left(-\frac{\Delta t - t_0}{\tau_2}\right), & \Delta t \geq t_0 \end{cases} \tag{E.1}$$

Here, I_{01} accounts for the constant PE intensity before photoexcitation ($\Delta t < t_0$) and I_{02} accounts for an intensity offset at the maximum investigated delay caused by long-lived spectral changes. At the time t_0, excited carrier population and depopulation dynamics set in. They are modeled using a sum of two exponential functions describing an exponential rise ($A_1 < 0$) and decay ($A_2 > 0$) of the transient PE intensity with time constants τ_1 and τ_2, respectively. To account for the temporal resolution Δt_{FWHM} of the experiment, the fitting function was convolved with a Gaussian function $g(t)$:

$$g(t) = \exp\left(-\frac{4 \cdot \ln 2 \cdot t^2}{\Delta t_{\mathrm{FWHM}}{}^2}\right). \tag{E.2}$$

Analog fit functions were used to account for the hot carrier response in the peak energy $E_{\mathrm{band}}(\Delta t)$ and peak width $\Delta E(\Delta t)$ transients.

For most cases, Eq. E.1 is appropriate to account for the dynamics associated with the hot carrier processes. As an example, Fig. S.3(a) shows the PE intensity transient for ROI A in Fig. ??(c) of the main text and the corresponding fit using equation E.1. However, in regions near E_{F}, we observed deviations from a pure exponential signal decay, including
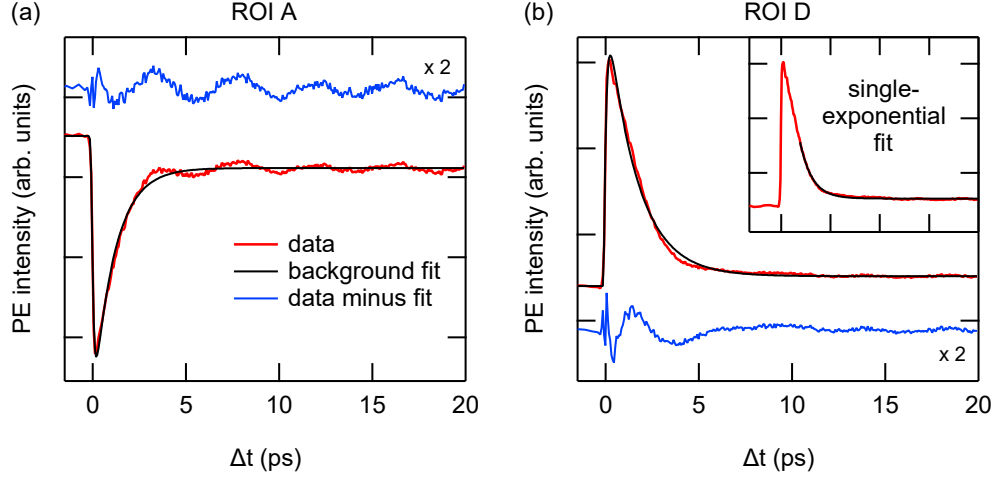
Supplementary Fig. S.3. Subtraction of hot carrier contribution. (a) PE intensity transient from ROI A (red) including a fit to the data starting at $\Delta t = -1.5\,\mathrm{ps}$ according to Eq. E.1 (black line). The blue line shows the PE intensity transient after subtraction of the fitting result. (b) Same as (a) for ROI D. The inset shows the same PE intensity transient including a single exponential fit starting at $\Delta t = 2\,\mathrm{ps}$.

the Weyl point region [ROI D, cf. Fig. **??**(d) of the main text]. The PE intensity transient from this region is shown in Fig. S.3(b) including the result of a fit using equation E.1. The deviation from an exponential decay is clearly visible and results in a signal distortion at small delays in the hot carrier-corrected data shown as blue line. The quality of the background subtraction procedure can be improved for this type of data by restricting the delay range to $\Delta t > 2\,\mathrm{ps}$ and by describing the hot carrier processes with a single exponential fit function. Still, a complete removal of hot carrier contributions is not possible resulting in a residual signal visible as a distortion in Fig. **??**(d) between $\Delta t = 5\,\mathrm{ps}$ and $\Delta t = 10\,\mathrm{ps}$.

SUPPLEMENTARY NOTE 4: COMPILATION OF FOURIER MAPS

For the energy- and momentum-resolved Fourier analysis of the data, the ARPES intensity maps were divided into small integration regions with a size of $23\,\mathrm{meV} \times 0.01\,\text{Å}^{-1}$. Each of these regions features a PE intensity transient showing a superposition of carrier population dynamics and coherent phonon-induced oscillations. Some spectral regions show an additional signal confined to the delay range around time zero [cf. Fig. **??**(d) and **??**(e)
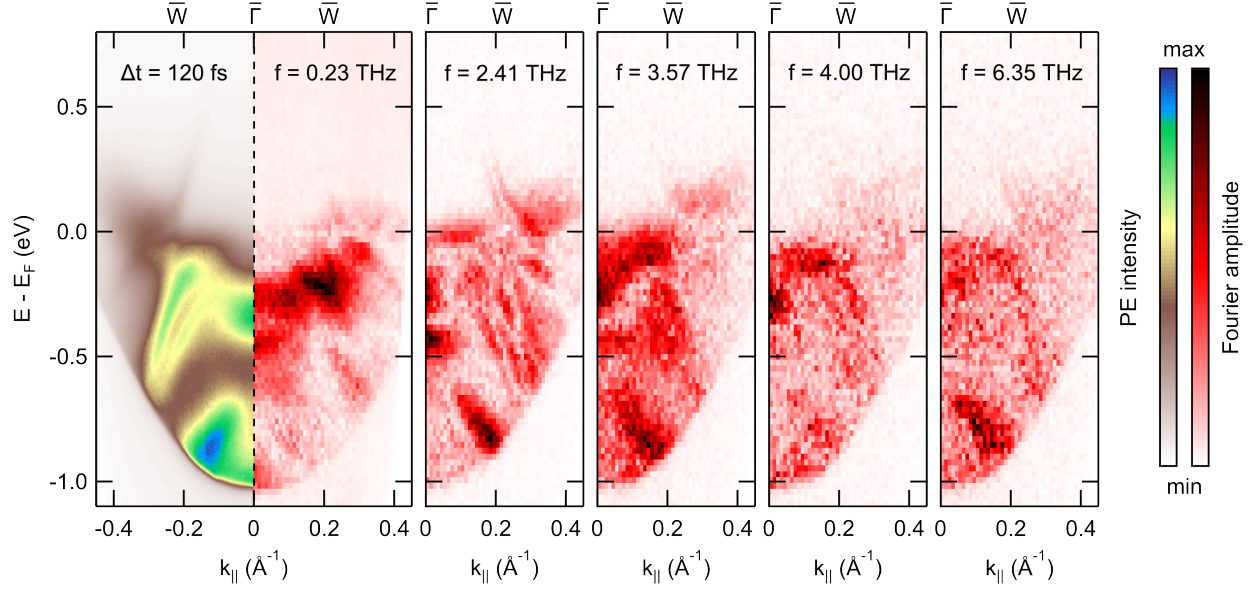
Supplementary Fig. S.4. Phonon mode-selective Fourier amplitude analysis of the TRARPES data. ARPES intensity map at $\Delta t = 120\,\text{fs}$ in comparison to Fourier maps of the five phonon frequencies identified in the Fourier amplitude spectra.

of the main text] that we assign to the pump-probe laser cross-correlation. We therefore restricted the data range for the analysis to a time delay range starting well after this signal contribution. Before the Fourier transformation, the PE intensity transients from each region were fitted for background subtraction with a single-exponential function to account for the carrier relaxation dynamics. The $3\,\text{ps}$ range data were analyzed for a delay range starting at $\Delta t = 280\,\text{fs}$. In the case of the $20\,\text{ps}$ range data, we had to exclude the first $2\,\text{ps}$ after time zero as a single-exponential fit of the intensity transients especially around the Fermi level results otherwise in low-frequency artifacts that interfere with the $0.23\,\text{THz}$ oscillation [see intensity transient of ROI D shown in Fig. S.3(b)].

After subtraction of the single-exponential background, the resulting transients were zero-padded to triple their lengths before their amplitude spectra were determined via fast Fourier transformation. This results in an energy- and momentum-dependent data set of Fourier amplitude spectra. A cut through this data set at a fixed frequency represents the energy- and momentum-resolved Fourier amplitude at the selected frequency. It can be displayed as a color-coded image which we refer to as Fourier map. Phonon-mode selectivity is achieved by selecting the frequencies corresponding to the coherent phonon modes. As an extended

version of Fig. **??** in the main text, Fig. S.4 shows Fourier maps at 0.23 THz, 2.41 THz, 3.57 THz, 4.00 THz, and 6.35 THz in comparison to the excited state ARPES intensity map at $\Delta t = 120$ fs. The 0.23 THz Fourier map results from the analysis of the 20 ps range data. In contrast, the four high-frequency Fourier maps are derived from the 3 ps range data.

We finally would like to add that the details of the Fourier map patterns critically depend on the type of spectral changes in the ARPES data that are induced by the coherent phonon excitation. In general, a pure periodic modulation in the PE intensity results in a slowly varying Fourier amplitude in the energy and momentum range of the signal modulations. In contrast, changes in peak energy or peak width result in distinct minima in the Fourier amplitude right at the peak position and Fourier amplitude maxima on both sides next to the peak. These effects are best seen when comparing the 0.23 THz and 2.41 THz Fourier maps. As discussed in the main text, the oscillations in the 0.23 THz data predominantly arise from pure PE intensity modulations resulting in a rather smooth Fourier map pattern. In contrast, the 2.41 THz Fourier amplitude shows a distinct fine structure of amplitude mimima that are indicative for shifts in the band energies or changes in the band widths in response to the excitation of the 2.41 THz phonon mode.

SUPPLEMENTARY NOTE 5: TIME-DEPENDENT FOURIER AMPLITUDE AND PHASE ANALYSIS

A time-dependent Fourier amplitude analysis enables us to gain information on the lifetime of the different coherent phonons and to identify possible mode frequency shifts as a function of time. Furthermore, a time-dependent Fourier phase analysis of phonon-induced band shifts allows for conclusions on the underlying excitation mechanisms of the coherent phonons, i.e., the distinction between a displacive excitation (DECP) scenario [**?**] and an impulsive stimulated Raman scattering (ISRS) excitation scenario [**?**].

Figure S.5 shows results of a time-dependent amplitude and phase analysis of the band energy transient of the prominent feature centered at $\bar{\Gamma}$ and $E-E_{\mathrm{F}} \approx -0.3$ eV in the ARPES intensity maps. The data comprise the frequency range of the four high-frequency coherent phonon modes, which periodically modulate the peak energy as discussed in the main text [cf. Figs. **??**(b) and **??**(c)]. For a time-dependent analysis, we successively shortened the band energy transient shown in Fig. **??**(b) of the main text at its beginning and performed
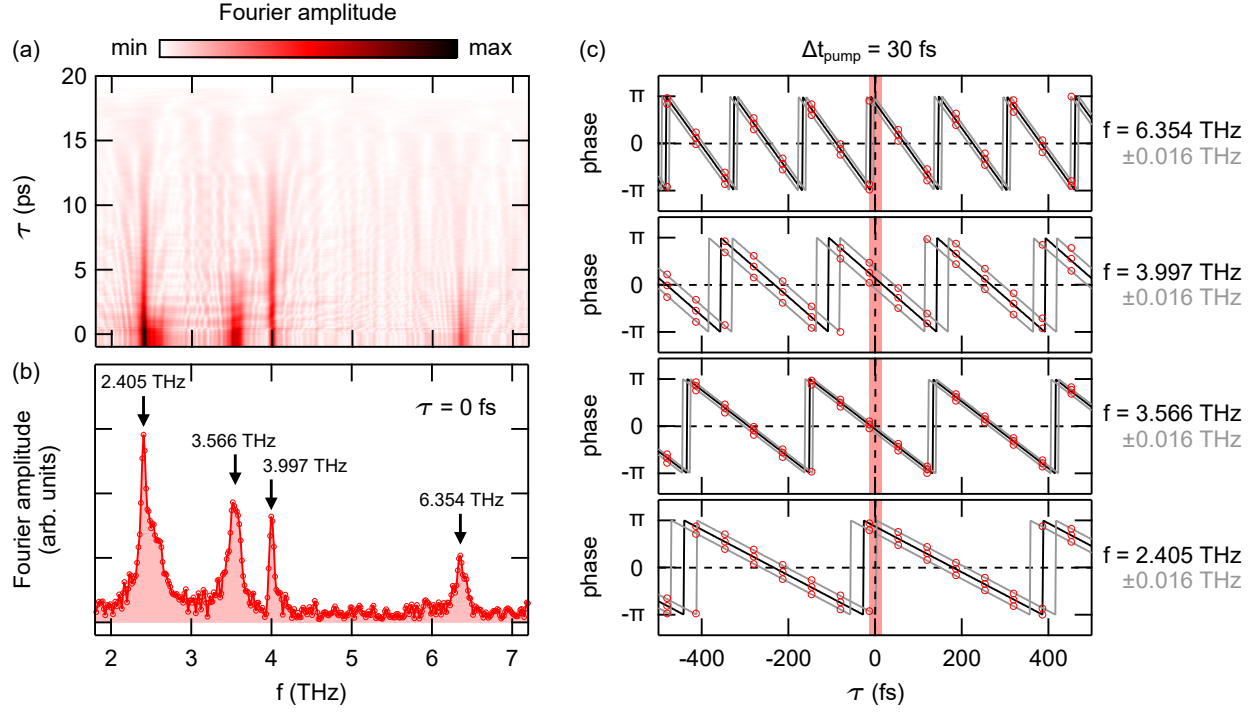
Supplementary Fig. S.5. Time-resolved Fourier amplitude and phase analysis of the high-frequency modes. (a) Fourier amplitude as a function of frequency and starting point τ of the band energy transient shown in Fig. **??**(b) of the main text. Details on the evaluation of the data are given in the text. (b) Fourier amplitude spectrum extracted from (a) for $\tau = 0\,\mathrm{fs}$. (c) Fourier phase as a function of τ for the peak positions of the four high-frequency modes. The black and gray lines show fits of a sawtooth function to the peak maximum data and the data of neighboring frequencies, respectively. The red shaded area at $\tau = 0\,\mathrm{fs}$ indicates the uncertainty in determining the time zero of the experiment due to the temporal width of the pump pulse.

a Fourier transformation of the remaining transient, respectively. Fig. S.5(a) displays the resulting Fourier amplitude as a function of frequency and starting point τ of the analyzed transient. The results illustrate the distinct differences in the lifetimes of the different modes, which obviously also conform with their differences in spectral width. The 3.57 THz mode and the 6.35 THz mode become damped within less than 6 ps, whereas the 2.41 THz mode and the 4.00 THz mode are still visible at 12 ps. For the 2.41 THz mode, we additionally observe a fast decaying shoulder which may hint to the excitation of a neighboring short-living coherent phonon. The data do not show any indications for a spectral shift of the modes as a function of time.

Figure S.5(b) shows the Fourier amplitude spectrum for $\tau = 0\,\mathrm{fs}$ extracted from Fig. S.5(a). We used this spectrum to determine the positions of the peak maxima (indicated in the figure by the arrows) for which we performed a time-dependent Fourier phase analysis. The results of the phase analysis are shown in Fig. S.5(c). We additionally performed a phase analysis for the data points next to the positions of the peak maxima at $\pm 0.016\,\mathrm{THz}$ to estimate the error in the determined phase. All results are fitted with sawtooth functions with the amplitudes set to a value of π. The phases of the oscillations at time zero indicate the underlying phonon excitation mechanism. Time zero was determined from the peak position of the laser cross-correlation signal that is in part of the data visible during the temporal overlap of pump and probe pulse [cf. Fig. ??(d) and ??(e) in the main text]. Our analysis yields initial phases of $(0.87 \pm 0.14)\pi$ for the excitation of the 2.41 THz mode, $(-0.07 \pm 0.06)\pi$ for the excitation of the 3.57 THz mode, $(0.14 \pm 0.22)\pi$ for the excitation of the 4.00 THz mode, and $(0.85 \pm 0.12)\pi$ for the excitation of the 6.35 THz mode. Within the error bars and under consideration of the pump pulse width, these results are compatible with a cosinusoidal response of the band energies to the excitation of the coherent phonons implying for all cases a displacive excitation [?].

For the phase analysis of the low-frequency interlayer shear mode, we analyzed the band energy transient of ROI A′ as shown in Fig. ??(e) of the main text. In this case, the initial phase can be directly determined from a fit of the transient. Although overlaid with a laser cross-correlation PE signal around time zero, the oscillation can be clearly identified as sinusoidal [cf. black line in Fig. ??(e) of the main text], implying for this coherent phonon mode an impulsive excitation [?].

SUPPLEMENTARY NOTE 6: ESTIMATION OF THE SHEAR MODE AMPLITUDE

An approximate estimation of the shear mode amplitude in Td-WTe$_2$ resulting from the excitation with 827 nm pump pulses at an incident fluence of $110\,\mathrm{\mu J\,cm^{-2}}$ becomes possible under consideration of quantitative results on the shear displacement reported for excitation with 23 THz pulses in Ref. [?]. To account for the different excitation wavelengths, we first referenced our data to fluence-dependent data on the shear mode frequency reported in a TRR study of Td-WTe$_2$ using 800 nm pump pulses [?]. Corresponding data for THz
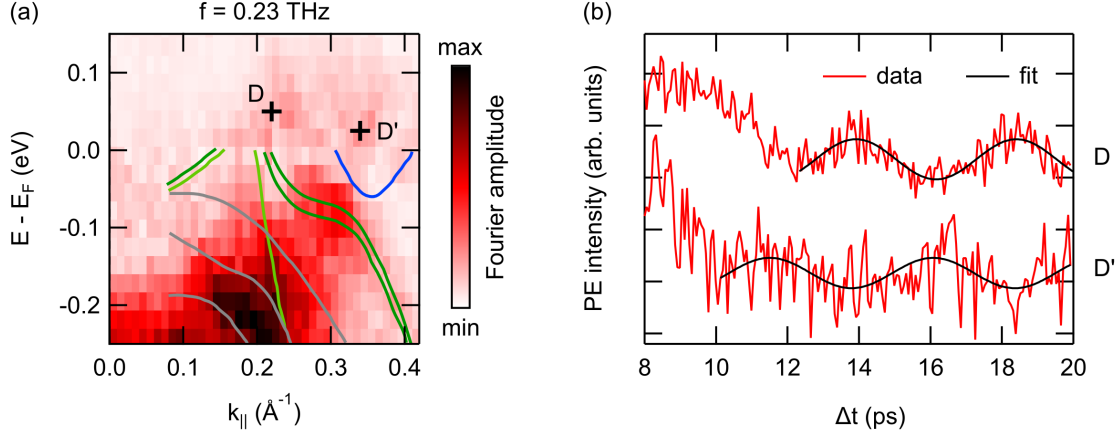
Supplementary Fig. S.6. PE intensity transients from energy-momentum areas above E_F. (a) 0.23 THz Fourier map with ROI D and ROI D' indicated. (b) Comparison of PE intensity transients from ROI D and ROI D'. The black lines are fits of a sinusoidal function to the data. For the analysis, we chose a signal integration area of $50\,\mathrm{meV} \times 0.025\,\text{Å}^{-1}$.

excitation as a function of the incident total pulse energy are also found in in Ref. [**?**]. Both studies report on an overall shift of the shear mode frequency of approximately 16 % over the probed pump fluence and energy ranges, respectively. Comparison of the data sets allow, therefore, to reference the 800 nm fluence values to the 23 THz pulse energy values. This comparison yields that the excitation with 800 nm, $150\,\mu\mathrm{J\,cm^{-2}}$ pump pulses results in a shear amplitude approximately corresponding to the excitation with 23 THz pump pulses with a field amplitude of $0.65\,\mathrm{MV\,cm^{-1}}$. Based on the quantitative discussion on the shear displacement in Ref. [**?**], this allows to roughly estimate the shear mode amplitude in our experiment to a value in the range of 1 pm. In this context, it is noteworthy that in Ref. [**?**] a complete annihilation of the Weyl points is predicted already for a shear displacement of 2 pm, even though the complete transition into the centrosymmetric $1\,T'(^*)$ phase requires an overall shear displacement of $\approx 12\,\mathrm{pm}$.

SUPPLEMENTARY NOTE 7: COMPARISON OF ROI ABOVE E_F

Figure S.6 compares PE intensity transients from the two energy-momentum areas above E_F that exhibit distinct amplitude maxima in the Fourier map at 0.23 THz. In Fig. S.6(a), the two areas (ROI D and ROI D') are indicated in the Fourier map, with ROI D already
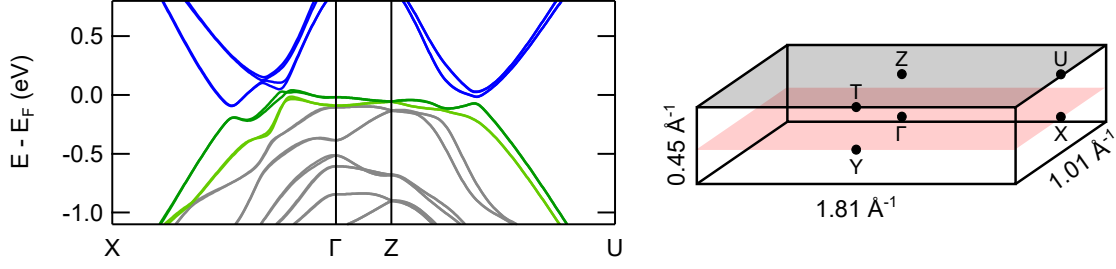
Supplementary Fig. S.7. Results of the band structure calculation of Td-WTe$_2$ for the Γ-X, Γ-Z, and Z-U direction. The 3D Brillouin zone of Td-WTe$_2$ is shown to the right.

introduced as the Weyl point area in the main text. The corresponding PE transients are shown in Fig. S.6(b). Whereas the signal from ROI D′ oscillates in phase with the signal from the ROI below E_F, ROI D shows a characteristic anti-phase behavior as already discussed in the main text.

SUPPLEMENTARY NOTE 8: BAND DISPERSION ALONG Γ-Z

In the main text, we discuss the potential relevance of the dispersion of the two low energy bulk bands along the Γ-Z direction. For comparison, we show in Fig. S.7 results of the band structure calculation for the Γ-X, Γ-Z, and Z-U direction. We used the same color coding for the bands as introduced in the main text.

REFERENCES